Journal of
Theoretical & Computational Science

Research Article　　　　　　　　　　　　　　　　　　　　　**Open Access**

Effect of Calcination Time on Structural, Optical and Antimicrobial Properties of Nickel Oxide Nanoparticles

Shanaj BR and John XR*

Department of Physics, Periyar EVR College (Autonomous), Tiruchirappalli, Tamil Nadu, India

Abstract

Nickel oxide nano crystallites were synthesized using Nickel [II] Chloride and Sodium hydroxide. The Thermo Gravimetric and Differential Thermo gravimetric (TGA/DTA) analysis were done to study the thermal behavior of the as synthesized sample Ni(OH)2. The peak at 290°C in DTA may be related to the decomposition of Ni(OH)2 into NiO. The structural, optical properties, morphology and composition of NiO nano particles (NPs) were studied by various techniques such as XRD, FTIR, UV-Vis, PL, FESEM and EDAX. The antimicrobial activity were carried out against Gram positive and Gram negative bacteria and NiO NPs showed inhibitory activity in both strains of bacteria with excellent selectivity against Gram-positive bacteria.

Introduction

The nanotechnology refers to hybrid science of chemical engineering and to a certain extent of Biology. The research in the area of nanostructure metal oxides have attracted extensive interest due to their novel optical, electronic, magnetic, thermal, catalytic and mechanical properties in comparison with their bulk materials [1,2]. Nickel oxide is a transition metal oxide, P-type semiconductor with a wide energy gap of 3.6 eV-4 eV [3]. It is used widely in manufacturing magnetic materials [4,5], alkaline battery cathodes [6], dye-sensitized solar cells, semiconductors, solid oxide fuel cells, anti-ferromagnetic layers [7], P-type transparent conducting films, electro chromic films, heterogeneous catalytic materials and gas sensors [8]. Currently some noble metal nanoparticles such as gold and silver are used as antimicrobial agents. In this context, nickel oxide nanoparticles are good alternative because they are more economical than gold and silver. These applications can be enhanced by decreasing the particle size in nano scale. In addition, nanoparticles with smaller size show good antibacterial activity [9]. However, NiO nanoparticles were previously reported as bactericidal and bacteriostatic agents.

Techniques used to synthesize nickel oxide nanoparticles have always been the scientific and technological interest. Several techniques, such as hydrothermal [10], sol-gel [11], solid-state reaction [12], electrochemistry [13], micro emulsions [14], spray pyrolysis [15,16] and precipitation [17] methods, have been developed to synthesize NiO nanoparticles.

In this article, a simple and cost effective co-precipitation method [18] was used to synthesis NiO nanoparticles. The influence of calcination time on structure, morphology, composition and photoluminescence property of NiO nanoparticles were investigated in detail and antimicrobial activity of NiO nanoparticles is tested against bacterial species using disc diffusion method.

Experimental Methods

Synthesis of nickel oxide nanoparticles

Nickel oxide nanoparticles have been synthesized by co-precipitation method and the block diagram is shown in Figure 1, 2.6 g of Nickel [II] Chloride (Aldrich, 98%) and 4 g of Sodium hydroxide pellets were dissolved in 100 ml of de-ionized water in two separate beakers. $NiCl_2$ solution was stirred by a magnetic stirrer for 2 hours. Then the NaOH solution was added to the $NiCl_2$ solution drop by drop under constant stirring. The resultant solution was kept at 70°C and stirred for 6 hours and was refluxed at room temperature for 24 hours. The resultant green precipitate was washed with double distilled water and ethanol to remove any possible ionic remnants if formed. The sample was dried by heating at 90°C in air and then calcined for different period of time (4 hr, 5 hr) at 700°C, the greenish sample turned into black color powder.

Characterization

The structure of the samples were analyzed by Powder X-Ray Diffraction (XRD) using X'Pert PRO Diffractometer using Cu K_α radiation of wave length 0.15406 nm in 2θ range of 10°-80° operated at 40 kV and 30 mA. Fourier transform infrared (FT-IR) spectra, UV-Vis spectra (Instrument model λ 35), Photoluminescence spectra (model-LS45) were recorded to analyze the functional groups and optical properties. Thermal property of as prepared sample were studied by Differential Thermal Analysis (DTA) and Thermo gravimetric Analysis (TGA 4000 Perkin Elmer). FESEM images display morphology and EDAX reveals the composition of NiO, NPs. The microbial strains used in the assay *Staphylococcus aureus* (MTCC 96), *Streptococcus pyogenes* (MTCC 102), Bacillus subtilis (MTCC 441), *Pseudomonas aeruginosa* (MTCC 741) and *Klebsiella pneumoniae* (ESBL-3971) were obtained from Microbial type culture collection (MTCC) at the institute of Microbial Technology (IMTECH), Chandigarh, India.

Antibacterial activity

AntibioGram was done by disc diffusion method, which is the most practical, low cost method for determining antibiotic susceptibility of microorganisms. A nutrient agar (NA) medium was prepared by

*Corresponding author: John XR, Department of Physics, Periyar EVR College (Autonomous), Tiruchirappalli-620 023, Tamil Nadu, India, Tel: +914312780286/+919443073908; E-mail: rj_xavier@yahoo.com
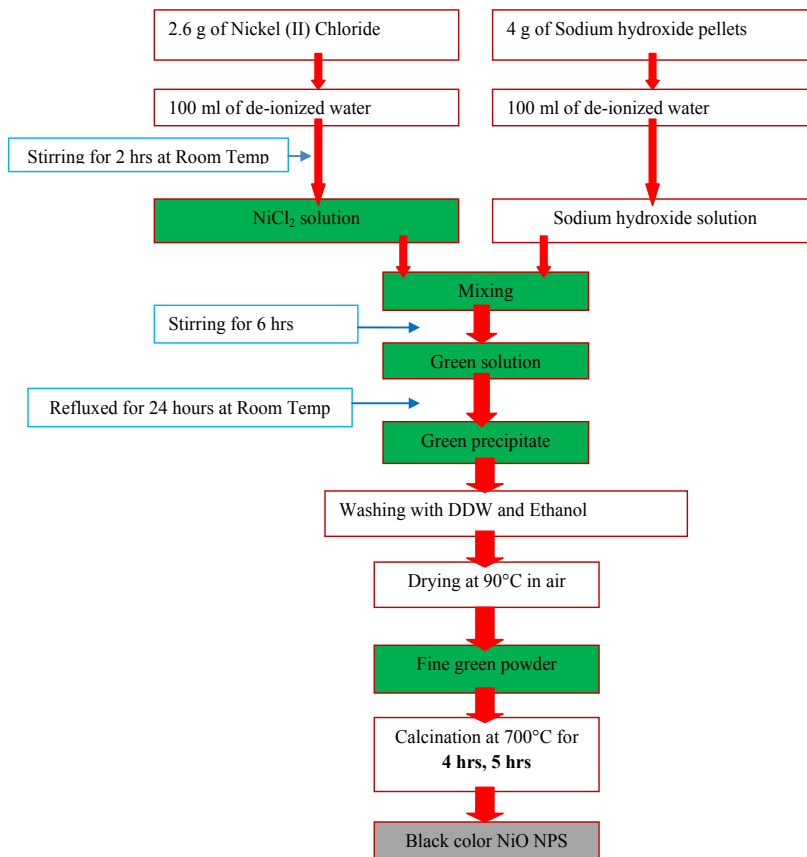
Figure 1: Block Diagram of Co-Precipitation method.

dissolving completely 28 g of nutrient agar in 1 L of distilled water and sterilized in autoclave at 121°C for 15 minutes. NA (30 ml) medium was poured into sterile Petri plates. The test organism was inoculated homogeneously on agar plates. A stock solution of NiO NPs was prepared in distilled water and using sterile forceps, discs (6 mm diameter) impregnated with the sample (50 μl, 100 μl, 150 μl) were dispensed on the surface of the inoculated agar plates and incubated at 37°C for 24 hr and at room temperature for 24-48 hr. Each sample was tested triplicate. The antibiotic diffusion from these discs into Agar medium leads to inhibition of bacterial growth. The antimicrobial potential of the calcined NiO samples was determined on the basis of mean diameter of the zone of inhibition around the disc which are measured and recorded in mm. Water was used as control sample. Chloramphenicol was used as the positive control against Gram positive (G$^+$) bacteria and Gram negative (G$^-$) to compare the efficacy of the test sample.

Results and Discussion

TGA and DTA analysis of Ni(OH)$_2$

Thermo gravimetric and the differential thermo gravimetric analysis of as synthesized Nickel hydroxide nanoparticles was carried out under Nitrogen atmosphere at a heating rate of 10°C/min in the temperature range of 35°C-750°C to investigate the thermal changes occurred during calcination (Figure 2). Three steps of weight loss are observed in the TG curve accompanied by three endothermic peaks in the DTG curve. A small endothermic peak observed around 55.6°C is due to the evaporation of residual water in dried sample. The other two sharp endothermic peaks located at 89.4°C and 290°C may be related

to the removal of water of crystallization and the thermo oxidative decomposition of Ni(OH)$_2$ respectively [19].

The thermal decomposition processes of Ni(OH)$_2$ can be represented as

$$Nicl_2 + 2NaoH \xrightarrow{\text{RT}} Ni(OH)_2 + 2NaCl \qquad (1)$$

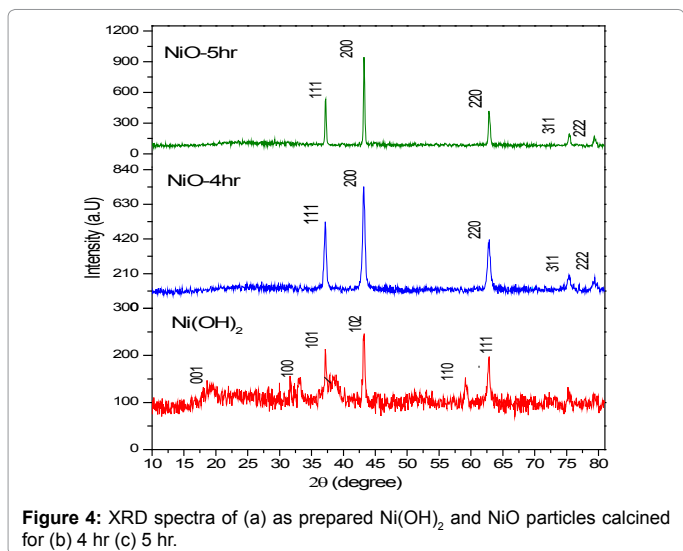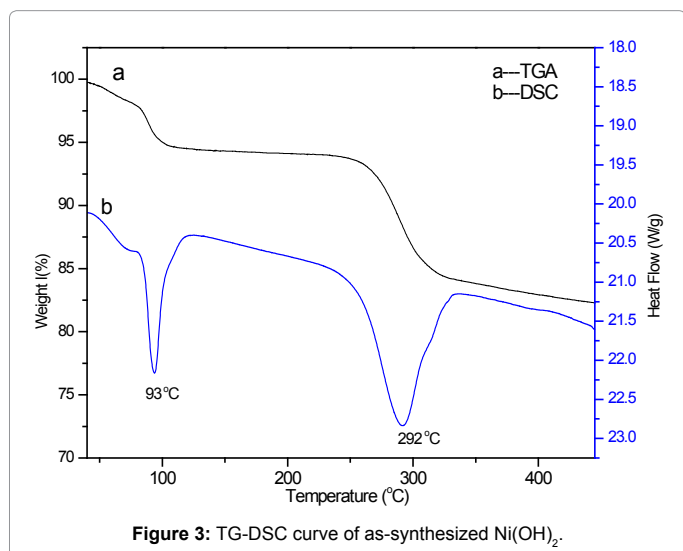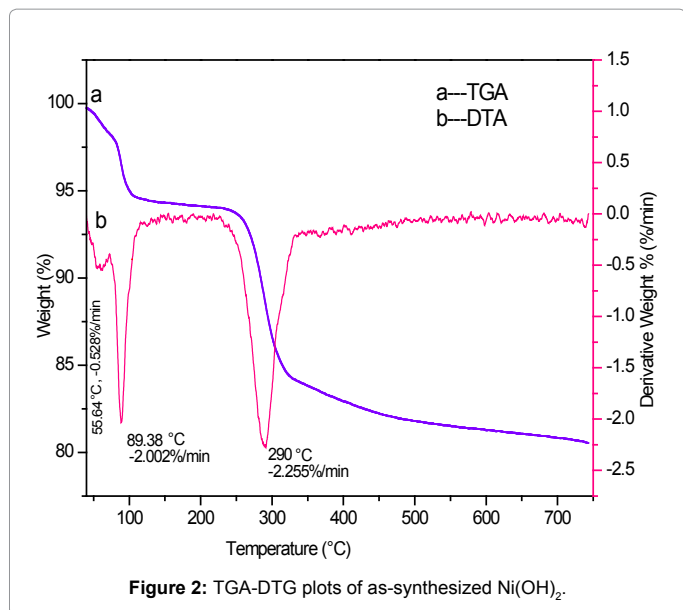$$Ni(OH)_2 \xrightarrow{290°C} NiOH + H_2O \qquad (2)$$
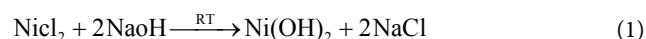
In the TGA curve, between 340°C and 700°C, the weight decreases slowly indicating the removal of a small amount of hydroxyl group during the conversion of the NiO phase. At 700°C, the weight loss of 19.192% is observed, which is very close to the stoichiometric weight loss 19.426% calculated from equation (2) for the removal of one H$_2$O molecule from Ni(OH)$_2$. Since the weight of the NiO measured from TG curve (i.e., 80.81%) is almost equal to calculated value (i.e., 80.56%), it is confirmed that the sample calcined at 700°C is pure.

DSC analysis of Ni(OH)$_2$

DSC analysis were also performed to measure the temperature and heat flow associated with transition in Nickel hydroxide sample from 0°C to 445°C at 10°C/min (Figure 3). The heating curve indicates that two strong endothermic peaks at 93°C and 292°C corresponds to crystallization and crystalline melt respectively which is in good agreement with DTA result.

XRD analysis

Figure 4 depicts XRD patterns of the as synthesized nano particles Ni(OH)$_2$ and NiO nanoparticles calcined for 4 hr and 5 hr. XRD pattern

Figure 2: TGA-DTG plots of as-synthesized $Ni(OH)_2$.

Figure 3: TG-DSC curve of as-synthesized $Ni(OH)_2$.

Figure 4: XRD spectra of (a) as prepared $Ni(OH)_2$ and NiO particles calcined for (b) 4 hr (c) 5 hr.

of $Ni(OH)_2$. Figure 4b is in good agreement with the standard pattern of $Ni(OH)_2$ and pattern reported for $Ni(OH)_2$ nanoparticles [20-22]. The observed peaks appreciably broad indicating that the as synthesized Nickel hydroxide nanoparticles are crystalline in nature with hexagonal phase.

XRD patterns of calcined NiO nano particles are shown in Figures 4b and 4c, respectively It is obvious that the well-defined peaks are indexed as (111, 200, 220, 311 and 222) that correspond to face-centered cubic (FCC) NiO phase which are in consistent with standard (JCPDS -file: 78-0429, Fm-3 m space group) data. It is observed that peaks are sharp with high intensity for higher calcinations time which means that bigger particle size may be generated by increasing the calcination time [23]. And also the Bragg's angles corresponding to the (hkl) planes shift slightly towards higher values indicate increase in crystallite size (Figure 5). The absence of any other peak illustrates the purity of samples. The size of the crystallite can be estimated using Debye- Scherrer formula [24].

$$D = \frac{K\lambda}{\beta} COS[\theta] \tag{3}$$

Where k=0.9, D is the size of the crystallite, λ is the wavelength of the Cu-Kα radiation (1.5406 Å), β is the full width at half maximum (FWHM) intensity and θ is the peak position. From the calculations, it is found that the average crystallite size of the as prepared sample $Ni(OH)_2$ is 25 nm, NiO (4 hr) is 22 nm, NiO (5 hr) is 42 nm. It is observed that increasing the calcination time from 4 hr to 5 hr leads to increase in crystallite size since crystallite growth is thermally accelerated.

It is always difficult to separate size and strain line boarding present in the XRD peaks. Williamson-Hall method [25] can be used to determine these two effects the by equation
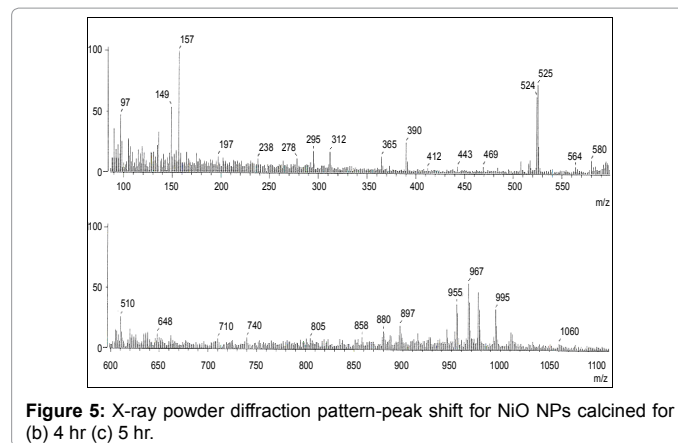
$$\beta Cos=[k\lambda/D]+4\varepsilon sin\theta \tag{4}$$

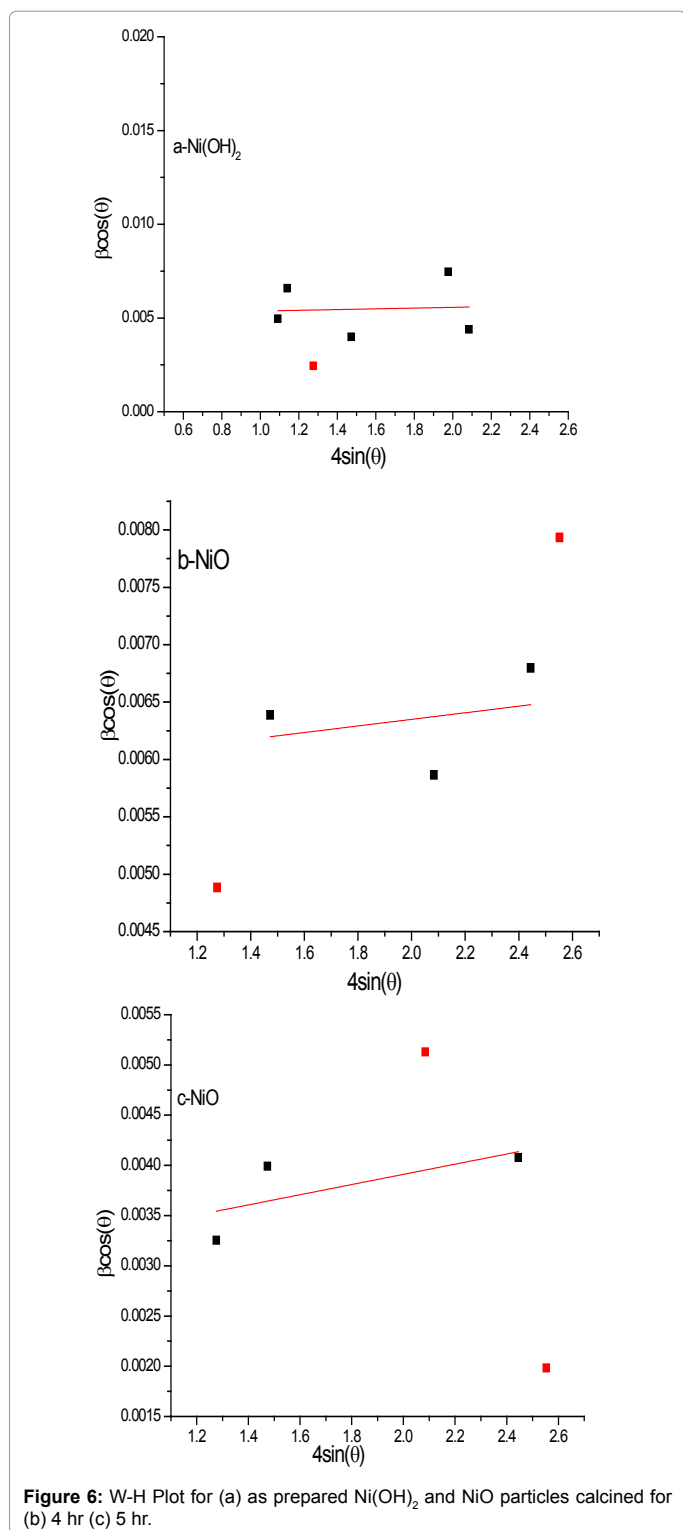Where k=0.9, ε is the strain, D represents the size of the crystallite. When we plot βcos versus 4sinθ, a linear fit is got. Strain (ε) and the size of the crystallite are calculated from the slope and y-intercept of the fitted line (Figure 6). The results are presented in Table 1. The crystallite size estimated from Scherer formula is found to be small due to peak broadening caused by micro strain and dislocations compared to the crystallite size obtained by WH analysis.

The micro strain [ε] induced in the samples due to imperfection and distortion is evaluated using the formula:

$$\varepsilon = \frac{\beta}{4 tan\theta} \tag{5}$$

Where β is the FWHM intensity and θ is the peak position (Table 1).

Figure 5: X-ray powder diffraction pattern-peak shift for NiO NPs calcined for (b) 4 hr (c) 5 hr.

Figure 6: W-H Plot for (a) as prepared Ni(OH)$_2$ and NiO particles calcined for (b) 4 hr (c) 5 hr.

The dislocation density (δ), which is defined as length of dislocation lines per unit volume of the crystal [26]. The dislocation density, which is a crystallographic defect within a crystal structure affects the properties of materials. It was also found that crystal with larger dislocation density were harder [27]. The dislocation density (δ) can also be determined using the expression

$$\delta = 1/D^2 \qquad (6)$$

Where D is the grain size in nm. The dislocation density and the micro strain of the as prepared sample Ni(OH)$_2$ and NiO nano particles synthesized at different calcination time are evaluated for maximum peak intensity (200) and the values shown in Table 2. It is concluded that the calcinations time increases from 4 hr to 5 hr the crystallite size increases, but the dislocation density and micro strain decreases. Using Bragg's law, the inter planer spacing between the atoms (d) is calculated. The lattice constant 'a' has been determined from inter planar spacing 'd' using the relation

$$d = a/[h^2 + k^2 + l^2]^{1/2} \qquad (7)$$

The crystallite size and value of 'd' calculated for maximum peak intensity (200) is as given in Table 2.

The lattice parameters estimated from the XRD patterns of the samples NiO (4 hr) and NiO (5 hr) are 4.187 Å, 4.184 Å respectively. It is clearly suggested that the increase of calcinations time results in decrease of lattice parameter. The lattice parameters calculated from XRD data are higher than that of standard lattice parameter 4.177 Å.

FT-IR analysis

Figure 7 shows the FT-IR spectra of as prepared sample Ni(OH)$_2$ and NiO nano particles after calcination at different period of time. In Figure 7a, a sharp peak at 3637 cm^{-1} is the characteristic of Ni(OH)$_2$ [28,29]. The broad absorption band centered at 3403 cm^{-1} is assigned to O-H stretching vibrations and the weak band at 1633 cm^{-1} is attributed to H-O-H bending vibration because of absorption of water molecules from air as the sample is synthesized in air. The band at 1017 cm^{-1} corresponds to C-O stretching bond [30]. The bands due to carbonate

Samples	Crystallite size (nm)		Dislocation density (δ) 10^{15} lines/m^2	Micro strain (ε)
	XRD	H Plot		
Ni(OH)$_2$	25	30	1.60	0.0078
NiO (4 h)	22	27	2.06	0.0034
NiO (5 h)	42	48	0.57	0.0020

Table 1: XRD parameter values for Ni(OH)$_2$ and NiO nano particles.

Figure 7: FTIR spectra of Ni(OH)$_2$ and NiO calcined for (b) 4 hr (c) 5 hr.
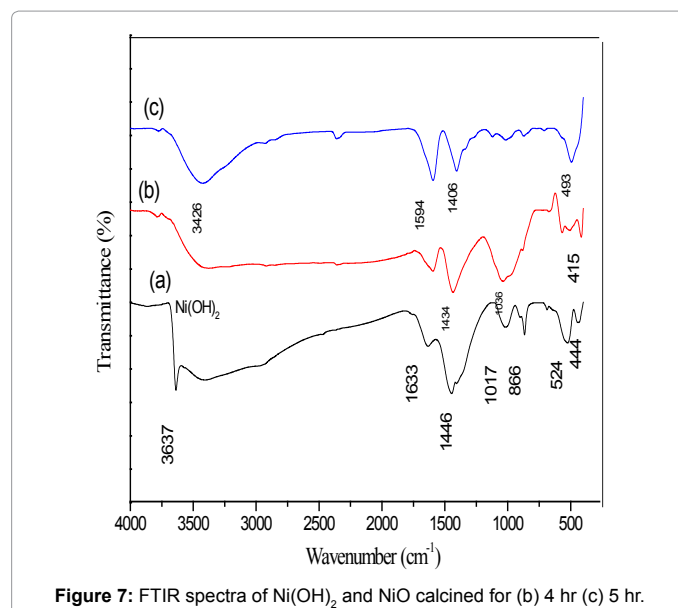
groups are observed at 1446 cm^{-1} and 866 cm^{-1}. The broad absorption bands at 524 cm^{-1}, 444 cm^{-1} are assigned to δ (O-H) and NiO stretching vibration mode.

When the sample is calcined for 4 hr, the main bands are observed at 3378 cm^{-1}, 1595 cm^{-1}, 1434 cm^{-1}, 1036 cm^{-1}, 882 cm^{-1}, 567 cm^{-1}, 415 cm^{-1} (Figure 7b). The bands at 3378 cm^{-1} is assigned to O-H stretching vibration and 1595 cm^{-1} are due to O-H-O bending vibration mode due to the fact that the calcined powder tend to absorb water. The bands due to carbonate groups and C-O stretching bond are observed at 1434 cm^{-1}, 882 cm^{-1} and 1036 cm^{-1} respectively. The appearance of new bands at 567 cm^{-1}, 415 cm^{-1} are assigned to Ni-O stretching vibration mode [31]. The broadness of the band indicates the nanocrystalline nature of the samples.

It is clear from Figures 7b and 7c that when the calcination time is increased, the same functional groups are appeared but intensity of the O-H band at 3426 cm^{-1} is increased which indicates that tendency to absorb water is increased. The absence of the peak at 3637 cm^{-1} reveals the complete transformation of Ni(OH)$_2$ into NiO nanoparticles. It is important to note that strong band exists at 493 cm^{-1} confirms the formation of NiO nanoparticles [32].

UV-Vis analysis

UV-Vis absorption spectra is used to study electronic structure of optical band gap of material. Figure 8 shows the optical absorption spectra of as prepared nanoparticles Ni(OH)$_2$ and NiO nano particles calcined for different period of time and the inset shows corresponding Tauc's plot. It is seen that the peak absorption intensity is found at 210 nm, 318 nm and 342 nm for the samples Ni(OH)$_2$, NiO (4 hr) and NiO (5 hr) respectively. When comparing the peak absorption wavelengths of calcined samples NiO (4 hr) and NiO (5 hr) a slight shift towards higher number is seen by increasing the calcinations time. This shift indicates a decrease in band gap, which can be attributed to increase in particle size [33].

The optical band gap is determined using Tauc's relation [34].

$$[Ah\nu]^n = k[h\nu - E_g] \qquad (8)$$

Where A is the absorbance is a material constant, E_g is the optical band gap energy of the material, hν is the photon energy and n depends on the type of transition; n is either 2 for direct band gap and ½ for indirect band gap. The graph of $[Ah\nu]^2$ as a function of hν is plotted for direct allowed transition. The linear portion of the curve is extrapolated to energy axis from which optical energy gap of the prepared and calcined samples are determined (Table 3). It is found that with the decrease in calcinations time, the band gap energy increases from 3.25 eV to 3.75 eV due to decrease in crystallite size which is an evidence of the quantum confinement effect.

Figure 9 shows UV-Visible transmittance spectra of the samples Ni(OH)$_2$, NiO (4 hr) and NiO (5 hr). It is seen that the optical transmittance of the NiO nanoparticles increases as calcinations time increases (Table 3).

Photo luminescence spectra

Pl spectra of Ni(OH)$_2$, NiO (4 hr) and NiO (5 hr) excited by 300 nm, 340 nm and 320 nm respectively is shown in Figure 10. It is observed that near band emission peaks exist at 339 nm, 357 nm, 365 nm for Ni(OH)$_2$, calcined NiO (4 hr) and NiO (5 hr), respectively. These emission peaks are due to electronic transition of Ni^{2+} ions [35]. Optical absorption study reveals the existence of several transitions at energies below band gap in NiO [36,37]. Adler and Frinleib [38] reported a series of absorption peaks below 4 eV as purely intra ionic 3d^8-3d^8 transitions of Ni^{2+} [39,40]. The PL results Table 4 revealed that
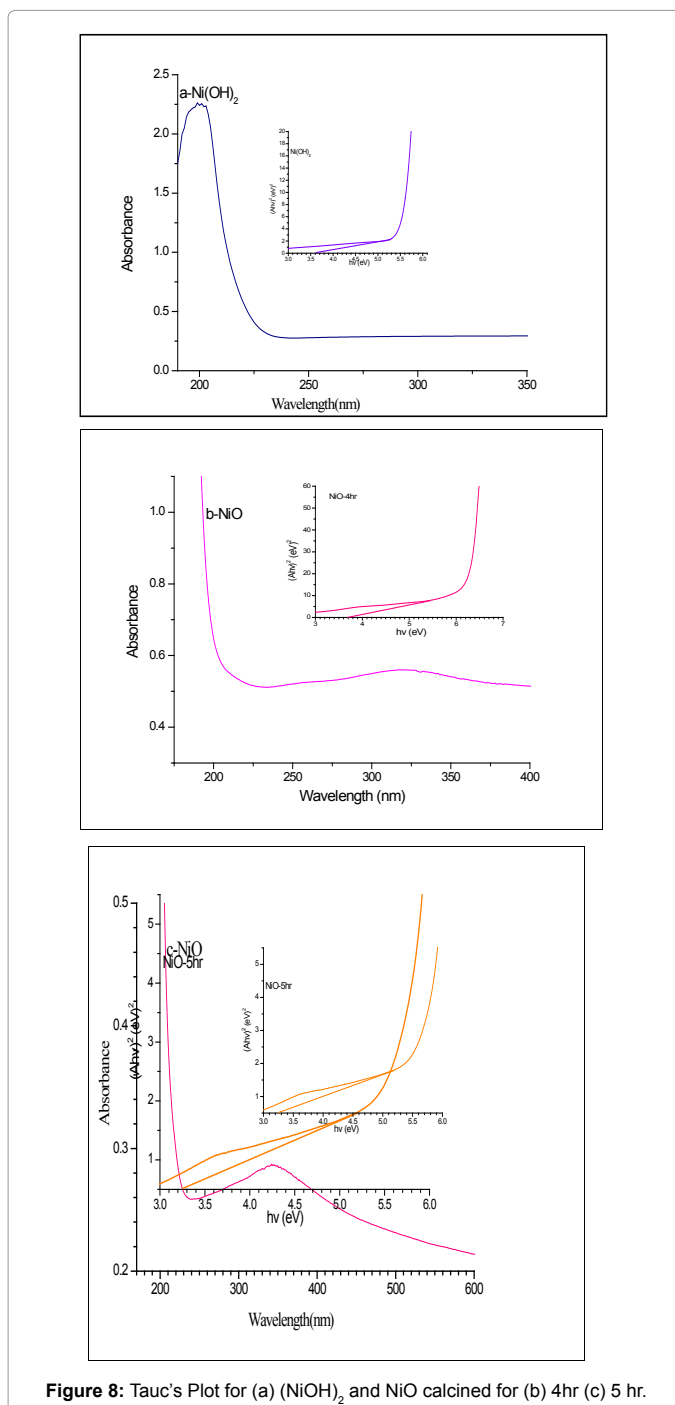

Figure 8: Tauc's Plot for (a) (NiOH)$_2$ and NiO calcined for (b) 4hr (c) 5 hr.

Samples	Position 2θ (°)	d-value (Å)		Crystallite size (nm)
		From XRD	Calculated	
Ni(OH)$_2$	43.1888	2.0947	2.0930	34
NiO (4 h)	43.1988	2.0943	2.0926	22
NiO (5 h)	43.2404	2.0924	2.0906	35

Table 2: Size and d-spacing of the Ni(OH)$_2$ and NiO nano particles at different calcinations time for maximum peak intensity.

Samples	Peak absorption wavelength (nm)	Tauc's Plot Band gap energy (eV)	Transmittance (%)
Ni(OH)$_2$	210	3.65	53
NiO 4 hr	318	3.75	31
NiO 5 hr	342	3.25	55

Table 3: Optical Parameters Ni(OH)$_2$ and NiO at different calcinations time.

Sample	Emission peaks (nm)	PL Intensity	PL Energy (eV)
(NiOH)$_2$	339	9.14	3.65
NiO- 4 hr	357	50.1	3.47
NiO- 5 hr	365	12.9	3.39

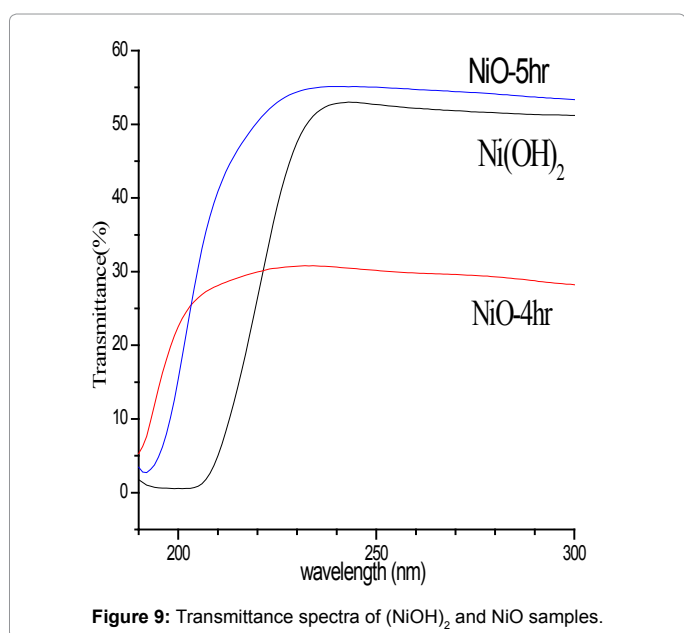**Table 4:** PL spectral data.

Figure 9: Transmittance spectra of (NiOH)$_2$ and NiO samples.
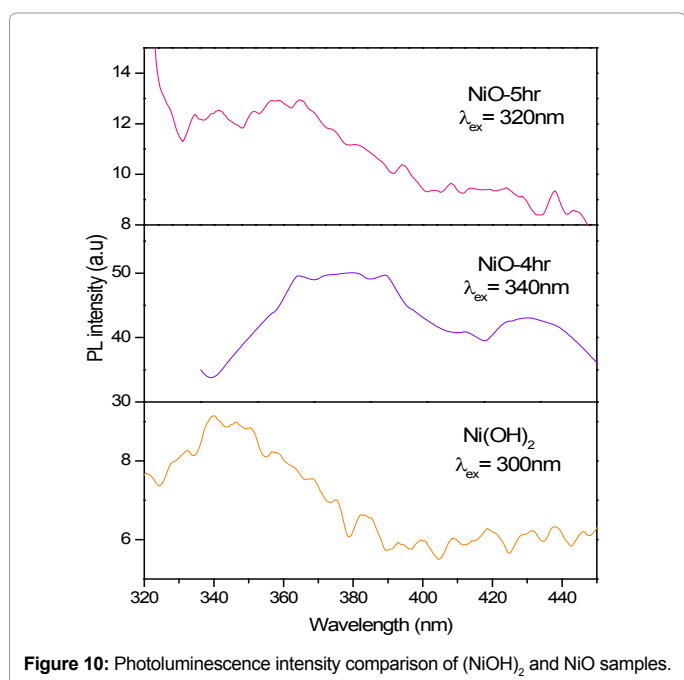

Figure 10: Photoluminescence intensity comparison of (NiOH)$_2$ and NiO samples.

as the calcinations time decreases, the particle size decreases but the PL intensity is enhanced. This can be explained as if the particle size is smaller, Oxygen vacancy is more and hence absorption of UV-Vis range increases which in turn causes stronger PL signal [41]. In all the samples blue or deep level emissions occur which can be related to defects such as Ni interstitials and Oxygen vacancies present in the sample.

Morphological and compositional studies

Figure 11 shows FESEM images of NiO (4 hr) NPs at different magnifications. It is observed that NiO nanoparticles are nearly spherical and cubical in shape. The aggregation of NiO nanoparticles is due to strong interactions. The average particle size was found to be in the range of 29 nm to 34 nm.

Figure 12 shows energy dispersive X-ray spectra (EDAX) of NiO (4 hr) nanoparticles used for elemental composition analysis. It indicates that the NiO nanoparticles are composed of Nickel (91.85%) and Oxygen (2.93%).

Antibacterial studies

Antibacterial activity of the NiO NPs calcined for 4 hr, 5 hr was tested against pure bacterial cultures of Gram positive (G+) (*S. aureus, S. pyogenes, B. subtilis*) and Gram negative bacteria (G-) (*P. aeruginosa, K. pneumonia*) and compared with Bacterial standard solution - Chloromphenical.

The photographic images of antimicrobial activity of calcined nickel oxide nanoparticles (4 hr, 5 hr) towards Gram positive and Gram negative bacteria are shown in Figure 13. The size of zone inhibition of the tested microorganisms by both the samples NiO (4 hr) and NiO (5 hr) at various concentrations against Gram positive and Gram negative bacteria. Figure 14 indicate that the antibacterial effect increases as NiO NPs concentration increases from 50 μl to 150 μl and the maximum zone of inhibition was found in 150 μl for both the samples. The mechanism depends not only on the concentration of NiO NPs, it also depends on sensitivity of bacterial species. The increased antibacterial effect may be due to reactive radicals Ni^{2+} ions [42], released continuously in the solution [43], may be attached to the negatively charged bacterial cell wall due to electrostatic force. The strong adhesion of Ni^{2+} ions to the bacterial cells causes distraction of cell membrane [44-46] and hence antimicrobial efficacy at higher NPs concentration [47].

The positive control Chloromphenical exhibited zone of inhibition (mm) in the range of (12.09 ± 0.83) to (12.40 ± 0.86) and (11.83 ± 0.82) to (12.01 ± 0.90) for NiO (4 hr) and NiO (5 hr), respectively at 30 μl.

The antibacterial results also revealed that Gram positive bacteria are more susceptible to NiO nanoparticles as compared to Gram negative bacteria due to the difference in the cell wall structure. The cell wall of Gram positive bacteria is made of a thick layer of peptidoglycan, which is attached to teichoic acids that are unique to Gram positive bacteria and can be damaged more easily [48]. But in Gram negative bacteria, cell wall contains a thin peptidoglycan layer and an outer membrane, constructed from tightly packed lipopolysaccharide (LPS) molecules [49], which is selectively permeable and regulates the transport through the plasma membrane. This renders Gram negative bacteria less susceptible to NiO NPs [50,51].

It is also found that the activity of NiO NPs calcined for 4 hr against both bacterial species is more than that recorded for NiO NPs calcined for 5 hr. Many reports have shown that the antibacterial activity of NiO nano particles is size dependent [52-54]. Table 5 reveals that as the size of the NiO particle (4 hr) decreases, Specific surface area (SSA)
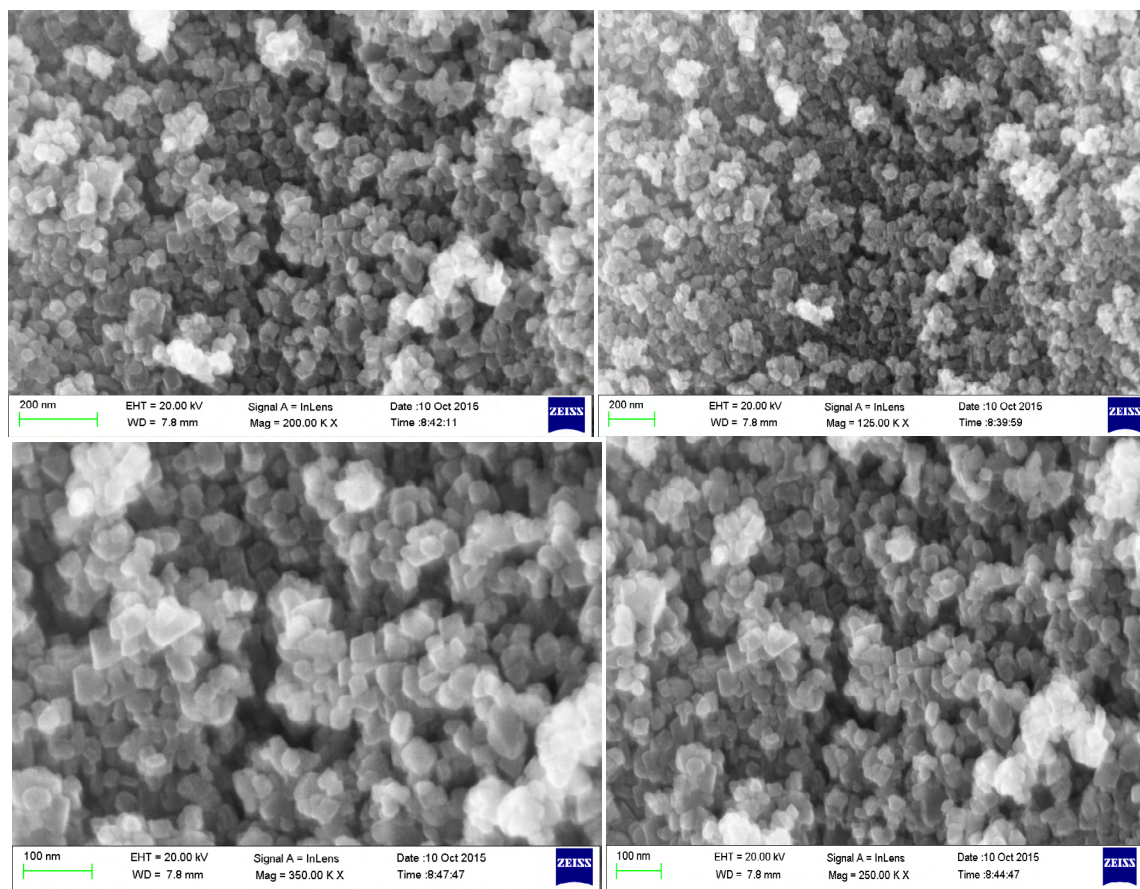
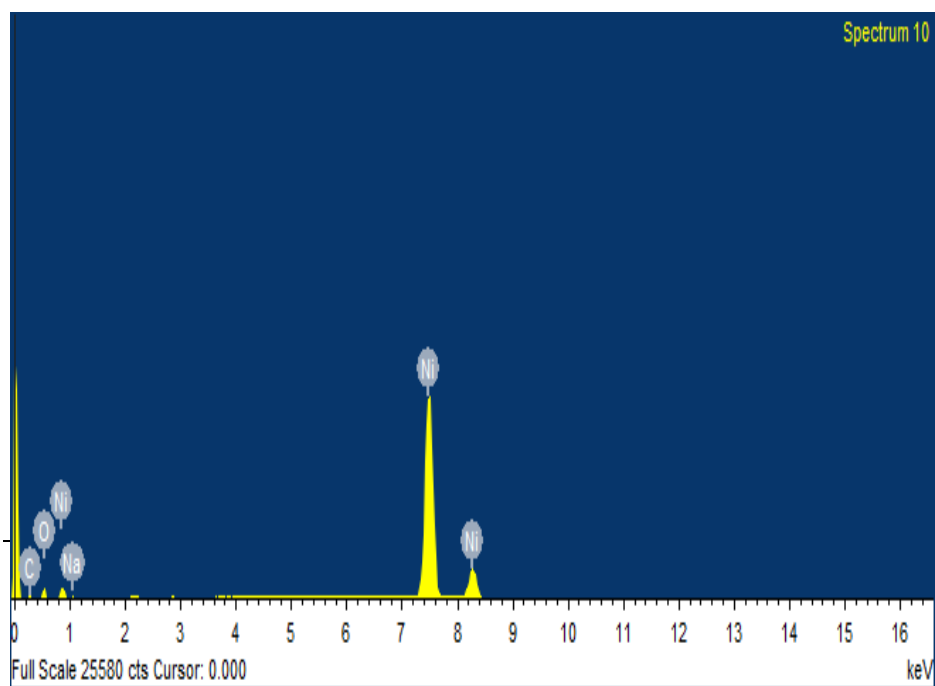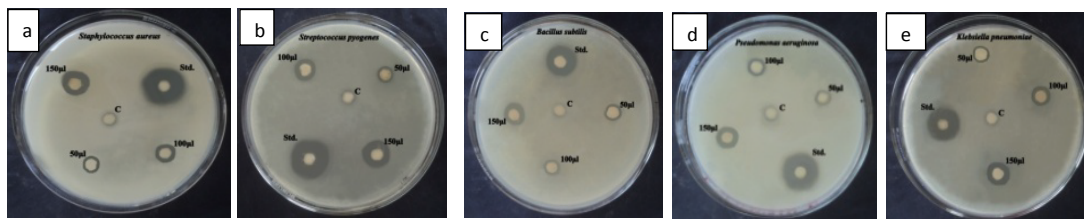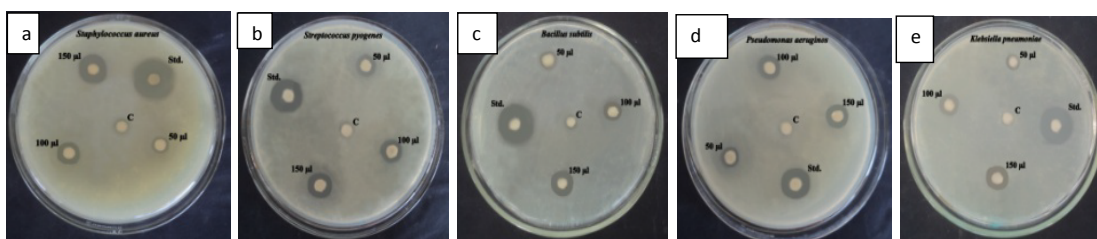**Figure 11:** FESEM images of NiO nanoparticles at different magnifications.

Figure 12: EDAX pattern of NiO nanoparticles.

A. Antibacterial activity of NiO – 4 hr

B. Antibacterial activity of NiO – 5 hr

Figure 13: Antibacterial activity of (A) NiO-4hr (B) NiO-5hr: Zone of inhibition of Nickel oxide NPs against Gram-positive bacteria (a) *S. aureus* (b) *S. pyogenes* (c) *B. subtilis* and Gram-negative bacteria (d) *P. aeruginosa* (e) *K. pneumoniae*.
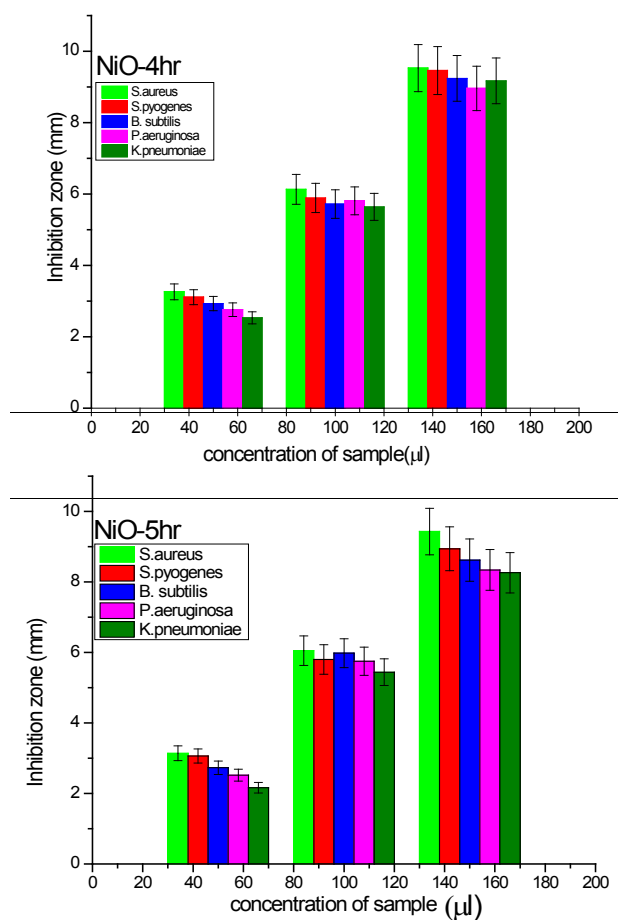

Figure 14: Bar graph shows the size of inhibition zone formed around each disc loaded with NiO sample, indicating the antibacterial activity towards both gram positive and gram negative bacteria. Error bars indicate standard deviation.

Samples	Average size D in nm	Surface Area $(nm)^2$	Volume $(nm)^3$	SSA (m^2/g)	SA: Volume
NiO-4 hr	22	1519	5572	41	0.273
NiO-5 hr	42	5538	38772	21	0.143

Table 5: Comparison of specific surface area of calcined samples.

and surface area to volume ratio increases, which play a vital role in interactions. The binding of small-sized NiO nanoparticles on the surface of the bacteria [55] react much faster with cell wall and generate reactive oxygen species (ROS) during the conversion of various nickel oxidedent based phases (NiO, NiOOH and $Ni(OH)_2$) to one another by dehydration/oxidation reactions [56] in aqueous media and this oxidative stress may ultimately cause damage to the membrane and kill bacteria [57-59]. This potential number of reactive groups on the particle surface results in the enhancement of antibacterial activities of NiO calcined for 4 hr.

Conclusion

Nickel hydroxide and Nickel Oxide NPs were successfully synthesized with high surface area by chemical precipitation method. TGA/DTA results show that the decomposition of Nickel hydroxide into Nickel oxide occurs at 290°C and the weight of the NiO measured from TGA curve at 700°C indicates that the sample is pure. XRD results confirmed that the increase in calcinations time resulted in increase in particle size with high surface area. The FTIR spectra illustrated the transformation of Nickel hydroxide into Nickel Oxide. UV-Vis absorption spectra revealed that increase in calcinations time produced a blue shift in the spectra, which led to decrease in energy gap with increase in particle size. PL spectroscopy studies showed that PL intensity decreases with the increase in calcinations time due to crystal growth. Based on results, it is concluded that particle size and optical properties are controlled by calcinations time. Hence, NiO nanoparticles can also be used in optoelectronic devices. The morphology and chemical composition were elucidated by FESEM and EDAX.

In this study the antibacterial activity of both the samples NiO (4 hr) and NiO (5 hr) were compared and the effect of NiO (4 hr) NPs having size 22 nm is excellent than NiO (5 hr) NPs having size 44 nm. It is also concluded that the antimicrobial property of NiO nanoparticles increased with increase in surface area to volume ratio due to decrease in particle size. Hence, smaller sized NiO nanoparticles can be used as an antimicrobial agent more effectively.

References

1. Li Q, Wang LS, Hu BY, Yang C, Zhou L, et al. (2007) Preparation and characterization of nanoparticles through calcination of malate gel. Materials Letters 61: 1615-1618.

2. Xin X, Lu Z, Zhou B (2007) Effect of synthesis conditions on the performance of weakly agglomerated nanocrystalline. J Alloys and Compounds 427: 251-255.

3. Chen HL, Lu YM, Hwang WS (2005) Characterization of sputtered NiO thin films. Surf Coat Technol 198: 138-142.

4. Ichiyanagi Y, Wakabayashi N, Yamazaki J, Yamada S, Kimishima Y (2003) Magnetic properties of NiO nanoparticles. Physica, pp: 862-863.

5. Makhlouf SA, Parker FT, Spada FE, Berkowitz AE (1997) Magnetic anomalies in NiO nanoparticles. J Applied Physics 81: 5561-5563.

6. Hotovy I, Huran J, Spiess L, Capkovic R, Hascik S (2000) Prepatation and characterisation of NiO thin films of gas sensor application. Vacuum 58: 300-307.

7. Bi H, Li S, Zhang Y, Du Y (2014) Int J Nanoscience and Nanotechnology 277: 363-367.

8. Hotovy I, Huran J, Spiess L, Hascik S, Rehacek V (1999) Preparation of nickel oxide thin films for gas sensors applications. Sens Actuators B Chem 57: 147-152.

9. Jones N, Ray B, Ranjit KT, Manna AC (2008) Antibacterial activity of ZnO nanoparticles suspensions on a broad spectrum of microorganisms. FEMS Microbiol Lett 279: 71-76.

10. Justin P, Meher SK, Rao GR (2010) Tuning of capacitance behavior of nio using anionic, cationic, and nonionic surfactants by hydrothermal synthesis. J Physical Chemistry 114: 5203-5210.

11. Mallick P, Sahoo CS, Mishra NC (2012) Structural and Optical Characterization of NiO nanoparticles synthesized by sol-gel route. AIP Conf Proc 1461: 229-232.

12. Wang WZ, Liu YK, Xu CK (2002) Synthesis of NiO nanorods by a novel simple precursor thermal decomposition approach. Chemical Physics Letters 362: 119-122.

13. Dierstein A, Natter H, Meyer F, Stephan HO, Kropf C, et al. (2001) Electrochemical Deposition under Oxidizing Conditions (EDOC): A New Synthesis for Nanocrystalline Metal Oxides. Scripta Materialia 44: 8-9, 2209-2212.

14. Han DY, Yang HY, Shen CB (2004) Synthesis and size control of NiO nanoparticles by water-in-oil microemulsion. Power Technology 147: 113-116.

15. Wang W, Itoh Y, Lenggoro IW, Okuyama K (2004) Nickel and nickel oxide nanoparticles prepared from nickel nitrate hexahydrate by a low pressure spray pyrolysis. Materials Science and Engineering: B 111: 69-76.

16. Bacaksiz E, Tomakin M, Altunbas M, Parlak M, Colakoglu T (2008) Structural, optical and magnetic properties of Cd 1-xCo xS thin films prepared by spray pyrolysis. Physica B 403: 3740 3745.

17. Karthik K, Selvan GK, Kanagaraj M, Arumugam S, Jaya NV (2011) Particle size effect on the magnetic properties of NiO nanoparticles prepared by a precipitation method. J Alloys and Compounds 509: 181-184.

18. Rahman A, Syed ahamed Haja H, Chandrasekaran K, Seemaisamy S, Venugopal Senthil K (2013) Impact of alkaline metal ions Mg2+, Ca2+, Sr2+ and Ba2+ on the structural, optical, thermal and antibacterial properties of ZnO nanoparticles prepared by the coprecipitation method. J Mater Chem B 1: 5950.

19. Alagiri M, Ponnusamy S, Muthamizhchelvam C (2012) Synthesis and Characterization of NiO nanoparticles by sol-gel method. J Mater Sci: mater Electron 23: 728-732.

20. De Wolff P (1972) The Standard Data Form for Powder Diffraction in Adobe Acrobat format.

21. Motlagh M, Kashani M, Youzbashi A, Sabaghzadeh L (2011) Int J Phy Sci 6: 1471.

22. El-Kemary M, Nagy N, El-Mehasseb I (2013) Nickel oxide nanoparticles: Synthesis and spectral studiesof interactions with glucose. J Materials Science in Semiconductor Processing 16: 1747-1752.

23. Rajesh K, Ashwani S, Nawal K, Narender B (2013) Preparation and Characterization of NiO Nanoparticles by Co-Precipitation Method. Int J of Engineering, Applied and Management Sciences Paradigms 6.

24. Alagar M, Theivasanthi T, Kubera Raja A (2012) Chemical capping synthesis of nickel oxide nanoparticles and their characterizations studies. J of App Sci 12: 398.

25. Nogi K, Hosokawa M, Naito M, Yokoyana T (2012) Nanoparticle Technology Book. 2nd edn. Kidiington, UK Elsivier.

26. Nehru LC, Swaminathan V, Sanjeeviraja C (2012) Photoluminescence Studies on Nanocrystalline Tin Oxide Powder for Optoelectronic Devices. American. J Mat Sci 2: 6-10.

27. Sirdeshmukh DB, Sirdeshmukh L, Subhadra KG (2006) Micro- and Macro-Properties of solids; Thermal, Mechanical and Dielectric properties. Springer, New York.

28. Motlagh M, Kashani M, Youzbashi A, Sabaghzadeh L (2011) Int J Phy Sci 6: 1471.

29. Abolanle Adekunle S, John Oyekunle A, Oluwatobi S, Oluwafemi, Abiodun Joshua O (2014) Comparative Catalytic Properties of $Ni(OH)_2$ and NiO Nanoparticles Towards the Degradation of Nitrite (NO2-) and Nitric Oxide (NO). Int J Electrochem Sci 9: 3008-3021.

30. Sharanabasava Ganachari V, Ravishankar B, Raghunandan, D Venkataraman (2012) Synthesis and characterization of nickel oxide nanoparticles by self-propagating low temperature combustion method. Recent Research in Science and Technology 4: 50-53.

31. Anandan K, Rajendran V (2011) Morphological and size effects of NiO nanoparticles via solvo thermal process and their optical properties. Materials Science in Semiconductor Processing 14: 43-47.

32. Anandha Babu G, Ravi G, Arivanandan M, Navaneethan M, Hayakawa Y (2013) Facile Synthesis of Nickel Oxide Nanoparticles and Their Structural, Optical and Magnetic Properties. Asian Journal of Chemistry 25: S39-S41.

33. Anandan K, Rajendran V. Structural, optical and magnetic properties of well-dispersed NiO nanoparticles synthesized by CTAB assisted solvothermal process. Int J Nanoscience and Nanotechnology.

34. Tauc J (1968) Optical properties and electronic structure of amorphous Ge and Si. Mater Res Bull 3: 37-46.

35. Anandan K, Rajendran V (2011) Morphological and size effects of NiO nanoparticles via solvothermal process and their optical properties. Mater Sci Semicond Process 14: 43.

36. Tsuboi T, Kleeman W (1994) Fine structure of near infrared optical absorption in NiO. J Phys: Condensed Matter 6: 8625.

37. Chakrabarty S, Chatterjee K (2009) Synthesis and Characterization of Nano-Dimensional Nickelous Oxide (NiO) Semiconductor. J Physical Sciences 13: 245-250.

38. Adler D, Feinleib J (1970) Electrical and Optical Properties of Narrow-Band Materials. Phys Rev B 2: 3112A.

39. Gorschluter, Merz H (1994) Localized d-d excitations in NiO(100) and CoO(100). Phys Rev B 49: 17293.

40. Fromme B, Moller M, Anschutz Th, Bethke, Kisker E (1996) Generalized Gradient Approximation Made Simple. Phys Rev Lett 77: 1548.

41. Sheena PA, Priyanka KP, Aloysius Sabu N, Boby Sabu, Thomas Varghese (2014) Effect of Calcination Temperature on the Structural and Optical Properties of Nickel Oxide nanoparticles-Nanosystems: Physics, Chemistry, Mathematics 5: 441-449.

42. Rishnamoorthy K, Moon JY, Hyun HB, Cho SK, Kim SJ (2012) Mechanistic Investigation on the Toxicity of MgO Nanoparticles toward Cancer Cells. J Materials Chemistry 22: 24610- 24617.

43. Morones JR, Elechiguerra JL, Camacho A (2005) Thebactericidal effect of silver nanoparticles. Nanotechnology 16: 2346-2353.

44. Wang X, Yang F, Yang W, Yang X (2007) A study on the antibacterial activity of one-dimensional ZnO nanowire arrays: effects of the orientation and plane surface. Chem Commun 14: 4419-4421.

45. Makhluf S, Dror R, Nitzan Y, Abramovich Y, Jelinek R, et al. (2005) microwave assays synthesis of nanocrystalline MgO and its use as a bacterioside. Adv Funct Mater 15: 1708-1715.

46. Sawai J, Microbiol J (2003) Quantitative evaluation of antibacterial activities of metallic oxide powders (ZnO, MgO and CaO) by conductimetric assay. Methods 54: 177-182.

47. Jadhav S, Gaikwad S, Nimse M, Rajbhoj A, Clust J (2011) Copper Oxide Nanoparticles: Synthesis, Characterization and Their Antibacterial Activity. Journal of Cluster Sci 22: 121-129.

48. Fu G, Vary PS, Lin CT (2005) Anatase TiO2 nanocomposites for antimicrobial coatings. J Phys Chem B 12; 8889-8898.

49. Zhen-Xing T, Bin-Feng LV (2014) MgO nanoparticles as antibacterial agent: Preparation and Activity. Brazilian Journal of Chemical Engineering 31: 591-601.

50. Mani Rahulana K, Padmanathanb N, Reji P, Balamurugand S, Kanakam CC (2013) Size determination of nickel oxide nanoparticles by electrochemical reduction method and its antibacterial activity. Appl Surface Sci 282: 656-661.

51. Tortora G, Funke RB, Case LC (2016) Microbiology: an introduction. Addison-Wesley.

52. Salah N, Habib SS, Khan ZH (2011) High-energy ball milling technique for ZnO nanoparticles as antibacterial material. Int J Nanomedicine 6: 863-869.

53. Jones N, Ray B, Ranjit KT, Manna AC (2008) Antibacterial activity of ZnO nanoparticles suspensions on a broad spectrum of microorganisms. FEMS Microbiol Lett 279: 71-76.

54. Raghupati KR, Koodali RT, Manna AC (2011) Size-dependent bacterial growth inhibition and mechanism of antibacterial activity of zinc oxide nanoparticles. Langmuir 27: 4020-4028.

55. Ghosh S, Ghosh D, Bag PK, Bhattacharya SC, Saha A (2011) Aqueous synthesis of ZnTe/dendrimer nanocompositesand their antimicrobial activity: implications in therapeutics. Nanoscale 3: 1139-1148.

56. Niklasson GA, Granqvist C, G Mater J (1956) Elementry of X-ray diffraction, Addison-Wesley Publishing company Inc., California.

57. Clutton S (1997) The importance of oxidative stress in apoptosis. Br Med Bull 53: 662-668.

58. Knaapen AM, Borm PJ, Albrecht C (2004) Schins RPL. Inhaled particles and lung cancer-Part A. Mechanisms. Int J Cancer 109: 799-809.

59. Kokkoris M, Trapalin CC, Kossionides S, Vlastou R, Nsouli B, et al. (2002) RBC and HIRBS studies of nanostructured AgSiO2 Sol-Gel thin coatings, ucl. Instr Meth Phys Res B 188: 67-72.